Importance of surface charging during plasma streamer propagation in catalyst pores

Importance of surface charging during plasma streamer propagation in catalyst pores

Quan-Zhi Zhang*, Wei-Zong Wang* and Annemie Bogaerts*

Research Group PLASMANT, University of Antwerp, Universiteitsplein 1, B-2610 Antwerp-Wilrijk, Belgium

Email: Quan-Zhi.Zhang@uantwerpen.be (Q.Z. Zhang), wangweizong@gmail.com (W.Z. Wang), annemie.bogaerts@uantwerpen.be (A. Bogaerts).

Abstract

Plasma catalysis is gaining increasing interest, but the underlying mechanisms are far from understood. Different catalyst materials will have different chemical effects, but in addition, they might also have different dielectric constants, which will affect surface charging, and thus the plasma behavior. In this work, we demonstrate that surface charging plays an important role in the streamer propagation and discharge enhancement inside catalyst pores, and in the plasma distribution along the dielectric surface, and this role greatly depends on the dielectric constant of the material. For $\varepsilon_r \leq 50$, surface charging causes the plasma to spread along the dielectric surface and inside the pores, leading to deeper plasma streamer penetration, while for $\varepsilon_r > 50$ or for metallic coatings, the discharge is more localised, due to very weak surface charging. In addition, at $\varepsilon_r = 50$, the significant surface charge density near the pore entrance causes a large potential drop at the sharp pore edges, which induces a strong electric field and results in most pronounced plasma enhancement near the pore entrance.

1. Introduction

Plasma catalysis is attracting considerable interest for environmental applications, such as gaseous pollutant removal and greenhouse gas conversion, as it combines the advantages of selectivity from catalysis and high reactivity from plasma technology [1-6]. However, the interaction between catalyst and plasma is rather complicated. On the one hand, the catalyst pellets/beads affect the plasma formation and propagation. Indeed, the electric field near the contact points is rather sensitive to the catalyst size, shape and dielectric constant, and it largely governs the plasma density and distribution [7-10]. In turn, the plasma distribution determines the effective contact area of the catalyst, and further affects its morphology or work function. Indeed, the work function of a catalyst is very sensitive to the surface conditions, and the plasma species affect the catalyst surface conditions by particle bombardment and surface reactions [1].

Some papers have reported that micro-discharges may be formed inside porous catalysts, either in between catalyst particles or inside the catalyst pores [11-13]. This is of crucial importance for plasma catalysis, as it determines the effective catalyst surface area exposed to the plasma species. By comparison with a non-porous catalyst, Holzer et al. [11-12] experimentally demonstrated that a porous catalyst yields a better reaction selectivity of hydrocarbon oxidation to CO_2, for volatile organic model compounds, and they provided the first experimental evidence for the presence of reactive plasma species in the interior of catalyst pores with a typical pore diameter of 10 nm [13]. In our previous work [14], we investigated the plasma penetration in catalyst pores with different diameter by a particle-in-cell / Monte Carlo collision (PIC/MCC) model, and we demonstrated that plasma streamers can only penetrate into catalyst pores when their diameter is larger than the Debye length.

Sharp edges and small sizes of the catalyst beads (or pellets) are typically reported to increase the decomposition and conversion rate [7, 9, 15], which was attributed to the enhanced electric field strength at the contact points between the beads or at the sharp edges near the catalyst pores [16-17]. Furthermore, experiments revealed that a large dielectric constant of the (catalytic or support) material typically leads to a higher CO_2 conversion [18] and decomposition efficiency of organic air pollutants [19]. Again, this was attributed to the electric field enhancement upon increasing the dielectric constant, both experimentally [19-21] and theoretically [8, 22-24]. Indeed, the dielectric material will be more effectively polarized at larger dielectric constant, so the electric field in the voids between the packing beads will be greatly enhanced, which affects the electron energy distribution function, and consequently the electron impact reaction rates. In addition, a transition in discharge mode from surface discharge to localised (point-to-point) filamentary microdischarge is observed [10, 25-26] upon increasing the material dielectric constant. Fluid modeling revealed that this was also attributed to the electric field enhancement at the contact points between the beads, which accelerates and directs the

electrons towards the beads. Hence, the electrons will not be able to spread out and the discharge becomes localised.

While the electric field enhancement is certainly a crucial factor in the above observations, all the papers mentioned above ignored the importance of surface charging along the surface of the beads (or the surface of catalyst pores), which is fairly sensitive to the material dielectric constant as well, and it may also affect the plasma behavior (including the electric field). In this work we will demonstrate that surface charging actually dominates the plasma distribution along the dielectric surface as well as the streamer propagation in the catalyst pores, and that it plays an important role in the discharge enhancement for different dielectric constants.

2. Computational Model

We apply a 2D implicit PIC/MCC model to study the plasma streamer evolution in a dielectric barrier discharge (DBD). The simulated cylindrical discharge geometry is 50 μm in height, and 90 μm in radius. The discharge is created in the gap between two electrodes, covered by a dielectric layer with thickness of 5 μm (bottom electrode) and 9.2 μm (top electrode). The geometry can be deduced from figure 1, which shows the streamer evolution with time. A small pore is created in the top dielectric layer for investigating the streamer propagation in the catalyst pore. The relative permittivity (dielectric constant) ε_r of the bottom dielectric has a fixed value of 4 (characteristic for SiO_2), while ε_r of the top dielectric varies between 4, 9, 25, 50, and 200 (characteristic for SiO_2, Al_2O_3, ZrO_2, TiO_2, and $CaTiO_3$, respectively [27]). The top electrode is grounded, while a negative DC voltage of -8 kV is applied to the bottom electrode. Atmospheric air is assumed as the discharge gas, with a constant density of background molecules (O_2, N_2) at 300K. A certain number of electron, N_2^+, O_2^+ and O_2^- super-particles are traced during the whole simulation. Each super-particle represents a group of real particles, and the number of real particles corresponding to a super-particle, is called weight ω_p. Initially, 20 super-particles of each species (electrons, N_2^+, O_2^+, and O_2^-) are placed right above the bottom dielectric as particle seeds with initial weight ω_p equal to 1, i.e., one super-electron corresponds to 1 real electron, and idem for the ions. Note that the mesh volume is very small, around 2×10^{-19} m^3, so this corresponds to an initial seed electron density of 10^{20} m^{-3}. A plasma streamer propagates from the bottom electrode towards the top electrode, and the electrons and ions will accumulate on the top dielectric surface, and thus contribute to surface charging. Besides a dielectric layer, we also perform simulations for a metallic coating on the top electrode (see below). The simulation region is uniformly divided into 1024 × 1800 cells, with a mesh size around 50 nm. The collisions included in the model are elastic collisions, excitation, ionization and attachment reactions of electrons with N_2 and O_2 gas molecules, like in [28]. The collision cross sections are adopted from the lxcat database [29]. A 'three-two' merging algorithm [30] is employed to restrict the number of particles: when the number of each type of super-particle exceeds 50 in each grid, three particles are combined into two particles with both conservation of momentum and energy. Correspondingly, the weight of particles will also increase. Photoionization is neglected in this study, because it is reported that the photoionization rate is much lower than the electron impact ionization rate [31], and the results are nearly the same with and without photoionization in a small gap of tens of μm [28].

3. Results and discussion

3.1 Plasma streamer evolution in the discharge gap

Figure 1 shows the plasma density distributions in the discharge gap at three different moments in time, from which the evolution of a plasma streamer can be revealed. As indicated in figure 1(a), the plasma streamer gradually develops from the avalanche of the particle seeds. Because the pore diameter (400 nm) is smaller than the Debye length in the streamer head, which is around 470 nm in this case (i.e. n_e ~1×10^{22} m^{-3}, T_e ~ 40 eV, this high electron temperature is caused by the strong local electric field (~10^8 V/m in the streamer head) and only appears in the streamer head), the plasma can only diffuse into the pore before the sheath is formed, which happens at around 8 ps. As soon as the sheath is formed, the plasma bulk is pushed away by the strong sheath potential, and the plasma will just spread out along the dielectric surface; hence no plasma can diffuse into the catalyst pore anymore. It should be noted that this behavior depends on the pore diameter, and when the pore diameter is larger than the Debye length in the streamer head, the plasma streamer can penetrate inside the catalyst pore, even when a sheath is formed, as demonstrated in [14] and as will be shown in the next section. A detailed

description of the plasma streamer evolution for pore diameters smaller than the Debye length can also be found in [14].

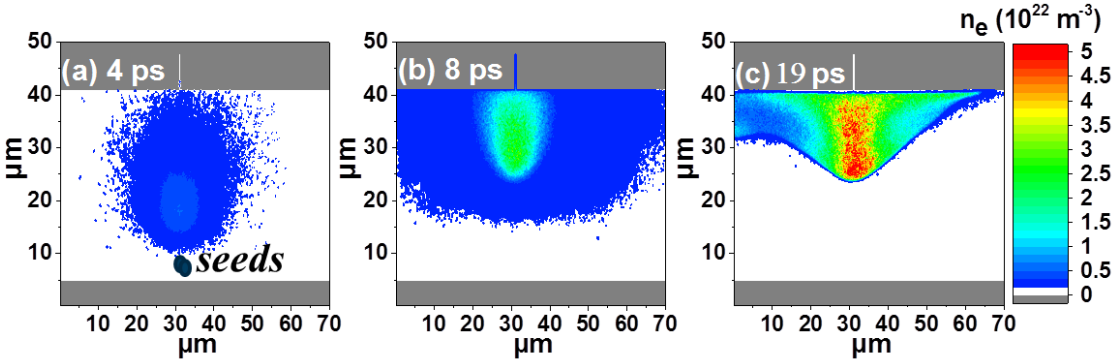

Figure 1. Plasma density distributions n_e (m^{-3}) at 4 ps (a), 8 ps (b), and 19 ps (c), illustrating the evolution of a plasma streamer inside the discharge. The pore in the top dielectric layer has a diameter of 400 nm. The dielectric constant ε_r is 4, but the same behavior is seen for dielectric layers with other dielectric constants. The left y-axis is the symmetry axis of the cylindrically symmetrical DBD.

Figure 2 shows the plasma density distributions at 19 ps for two other dielectric constants of the upper dielectric layer, to be compared with Figure 1(c). The plasma spreading along the dielectric is somewhat suppressed at increasing ε_r, or in other words, the plasma covers a wider region of the dielectric layer at smaller ε_r (i.e., with radius of 70 μm at $\varepsilon_r = 4$, 65 μm at $\varepsilon_r = 50$, and below 60 μm at $\varepsilon_r = 200$). This behavior corresponds with experimental and modeling results from literature [10, 24], in which the discharge becomes more localised upon increasing ε_r of the dielectric beads in a packed bed DBD reactor, with a discharge mode transition from surface discharges to localised micro-discharges. This phenomenon was explained by the enhanced electric field at the contact points between the beads, which is so strong that the electrons are accelerated and get lost on the surface of the beads, rather than having the ability to spread out over the surface [10, 24]. However, we will demonstrate below that surface charging is mainly responsible for the variation of the plasma distribution at dielectric surfaces with different dielectric constants.

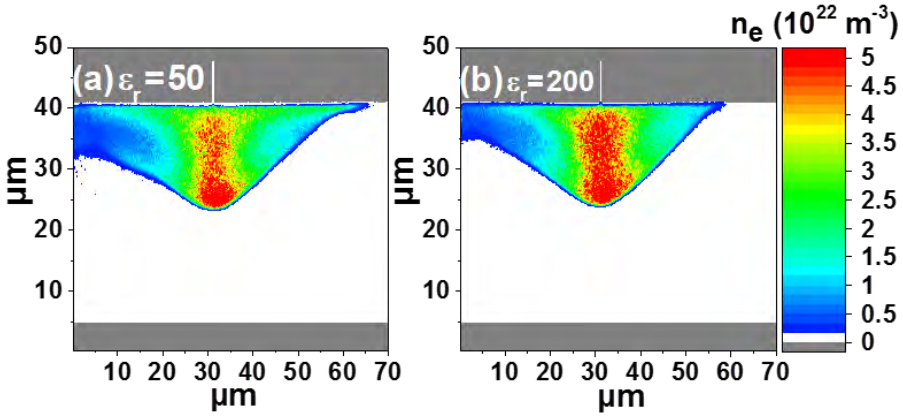

Figure 2. Plasma density distributions n_e (m^{-3}) at 19 ps, for an upper dielectric layer with dielectric constant ε_r of 50 (a), 200 (b). The pore has a diameter of 400 nm.

We also performed simulations when placing the seed particles off-center from the pore. In this case, the plasma streamer will first arrive at the dielectric and then develop along the surface due to the surface discharge. The plasma will further develop into the pore when the pore diameter is larger than the Debye length, and induce discharge enhancement inside the pore, following the same mechanism as explained above. However, since the surface discharge becomes very difficult for high ε_r, we performed all simulations for the paper by placing the seed electrons at the center below the pore.

3.2 Plasma streamer propagation in catalyst pores

Figure 3 illustrates the plasma density distributions near and inside a pore, for different pore diameters and different dielectric constants of the dielectric layer at the top electrode. The pore depth is fixed at 7 μm. We see a clear discharge enhancement inside the pore for almost all pore diameters and dielectric constants. This discharge enhancement is caused by the surface discharge along the pore sidewalls, as will be explained in detail below. The strongest discharge enhancement always happens for the 800 nm pore diameter, for the different dielectric constants. Furthermore, the maximum plasma density first increases when rising ε_r to 50, but then it decreases when further rising ε_r to 200. This trend is qualitatively in good agreement with the results in [32], predicted from fluid modelling, although the latter results were obtained for a helium discharge and much larger pore diameters (≥ 30 m), which is of lower interest for catalysis applications.

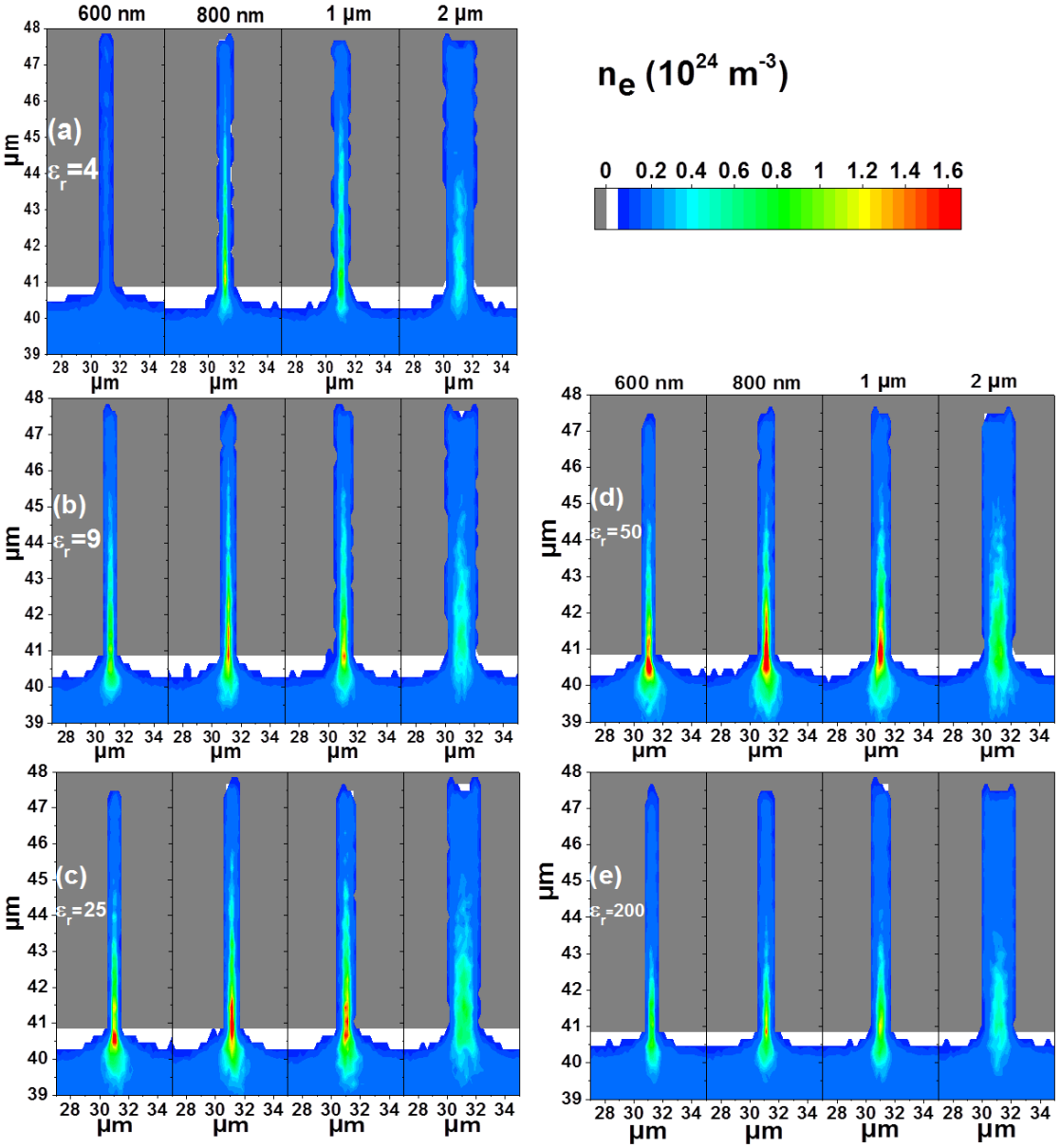

Figure 3. Plasma density distributions n_e (m^{-3}) at 19 ps, near and inside a pore with diameter of 600 nm, 800 nm, 1 μm, and 2 μm, for $\varepsilon_r = 4$ (a), $\varepsilon_r = 9$ (b), $\varepsilon_r = 25$ (c), $\varepsilon_r = 50$ (d), and $\varepsilon_r = 200$ (e).

It is worth to note that the length of the streamer slightly reduces upon rising ε_r. For instance, for the 800 nm pore, the streamer reaches till 46 m at $\varepsilon_r = 4$, till 45 m at $\varepsilon_r = 50$, and till less than 44 m at $\varepsilon_r = 200$. Thus, the plasma streamer propagation becomes more difficult for large ε_r. The reason is surface charging, as will be explained in the next section. This behavior is consistent with the reduced horizontal spreading of plasma in figure 2, and with the mode transition from surface discharges to localised micro-discharges in [10, 24], upon rising ε_r. However, the explanation put forward in [10, 24]

does not apply here. Indeed, the polarization inside the dielectrics will enhance the vertical space electric field between the dielectric electrodes. The electric field is now in the same direction as the streamer propagation, so we would expect that the electrons are accelerated towards the pore entrance and further towards the pore bottom, and that the streamer can propagate deeper at larger ε_r, according to the explanation in [10, 24], which is the opposite from the results in figure 3. Therefore, the enhanced electric field cannot explain the streamer propagation behavior inside catalyst pores with rising ε_r. In contrast, surface charging plays a crucial role in explaining this behavior.

3.3 Effect of surface charging during plasma streamer propagation

Figure 4 illustrates the surface charge density along the pore sidewalls, for different dielectric constants, at 19 ps, to reveal the mechanism of streamer propagation inside the pore. Since the plasma Debye length in the streamer head is around 470 nm for the different dielectric constants in this work, and the pore diameter is 800 nm, the streamer can easily enter the pore, as can indeed be deduced from the surface charging in figure 4. When the streamer arrives at the pore, the electrons will charge the pore sidewalls. The charging will be non-uniform as a function of depth, which will induce an extra (surface) electric field along the sidewalls. When ε_r is small, this extra surface electric field is so strong that the streamer is rapidly accelerated toward the pore bottom, and contributes to a further discharge enhancement due to a surface discharge. That is why the largest surface charge density appears at the pore bottom for $\varepsilon_r = 4$ and $\varepsilon_r = 9$ (see figure 4). When ε_r increases, the dielectric material can be more easily polarized, which will significantly reduce the surface electric field strength along the pore sidewalls. The streamer propagation thus slows down for larger ε_r. As a consequence, the surface charge density becomes relatively uniform along the pore sidewalls at $\varepsilon_r = 25$, and when $\varepsilon_r \geq 50$, the largest surface charge density appears near the pore entrance. Hence, the surface discharge becomes less pronounced deeper into the pore at larger ε_r (≥ 50). This explains the shorter streamer length inside the pore for larger ε_r, as illustrated in figure 3.

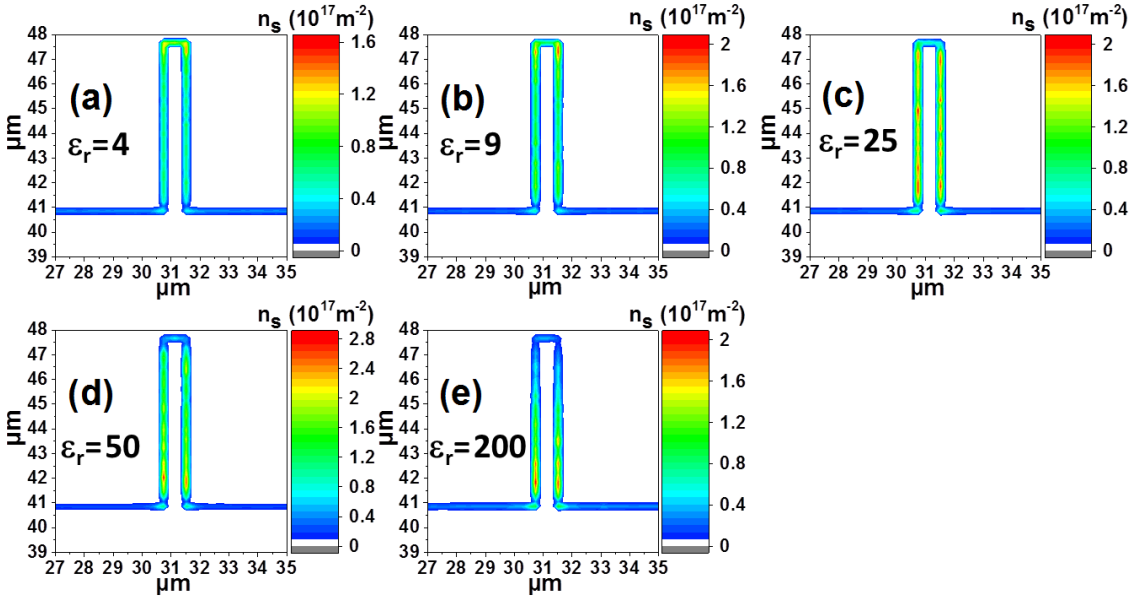

Figure 4. Absolute surface charge density n_s (m^{-2}) accumulated on the dielectric surface, near and inside a pore with diameter of 800 nm, and with ε_r of 4 (a), 9 (b), 25 (c), 50 (d), and 200 (e), at 19 ps.

The weaker surface electric field strength along the pore sidewalls upon larger ε_r can be deduced from the clearly lower electric potential drop across the entire pore depth in the top dielectric, as shown in figure 5 (upper panels a-c). At the same time, however, the sharp edges at the pore entrance always induce a large curvature in the potential distribution, as indicated by the dashed lines in figure 5 (lower panels d-f). These lower panels illustrate the same potential distributions, but in a narrower range to better indicate the details near the pore entrance. The potential drop near the pore entrance is around 120 V (i.e., from -1710 V to -1830 V) at $\varepsilon_r = 4$, around 150 V (from -610 V to -760 V) at $\varepsilon_r = 50$, and around 60 V (from -290 V to -350 V) at $\varepsilon_r = 200$. Furthermore, this potential drops over a shorter distance closer to the pore edge (see dashed lines), which induces a strong electric field (around

1.7×10^8 V/m at $\varepsilon_r = 4$, 4×10^8 V/m at $\varepsilon_r = 50$, and 2.5×10^8 V/m at $\varepsilon_r = 200$) near the pore edge, resulting in a high electron density near the pore entrance (shown in figure 3 above). This corresponds well with the enhanced electric field and increased decomposition and conversion rate in [7, 16-17] with packing beads of sharp edges. Thus, we may conclude that the stronger polarization at $\varepsilon_r = 50$ results in a weaker surface discharge along the pore sidewalls, and thus somewhat more limited streamer penetration towards the pore bottom, but at the same time the potential drop at the pore entrance is more curved than for $\varepsilon_r = 4$, due to a very large surface charge density at the pore entrance, inducing a stronger electric field at the pore edge. Consequently, the electron density is the highest at the pore entrance for $\varepsilon_r = 50$, as shown in figure 3 above.

When further increasing ε_r to 200, the polarization is much stronger, and the potential drop across the top dielectric becomes very small (see figure 5(c)), and it is also more limited near the pore entrance (60 V; see figure 5(f)), explaining why the electric field and consequently the electron density are not so enhanced at the pore entrance.

The influence of ε_r on the surface charging effect thus explains the trend of maximum plasma density with ε_r, i.e. it first increases and then decreases, as shown in figure 3. Therefore, we can conclude that the surface charging largely determines the plasma streamer propagation inside the catalyst pores. The surface discharge becomes less pronounced at $\varepsilon_r \geq 50$, which makes the discharge more localised, i.e., more electrons will accumulate near the sharp edge of the pore entrance. At moderate ε_r (~ 50), both the sharp edges and the concentrated surface charge density cause a strong potential drop and thus a significant electric field near the pore entrance, which explains the most pronounced discharge enhancement inside the pore for $\varepsilon_r = 50$.

It is worth to note that, for a moderate ε_r (around 50), the discharge tends to become localised. Indeed, the conductivity of the dielectric is very low, so the surface charging will continue accumulating with discharge evolution, and the electric field induced by the surface charging becomes more and more significant, but in the reversed direction with the applied electric field, which will keep affecting the following discharge, and even quench the plasma streamer. However, when ε_r becomes very high (>>200), although the discharge will become more localised, both the conductivity and polarization of the dielectric greatly increase, and the surface charge will not increase with discharge evolution, and thus the effect of surface charging will gradually become negligible. The condition of no surface charging can be revealed from the case of a metallic coating in next section, which is equivalent to infinite ε_r.

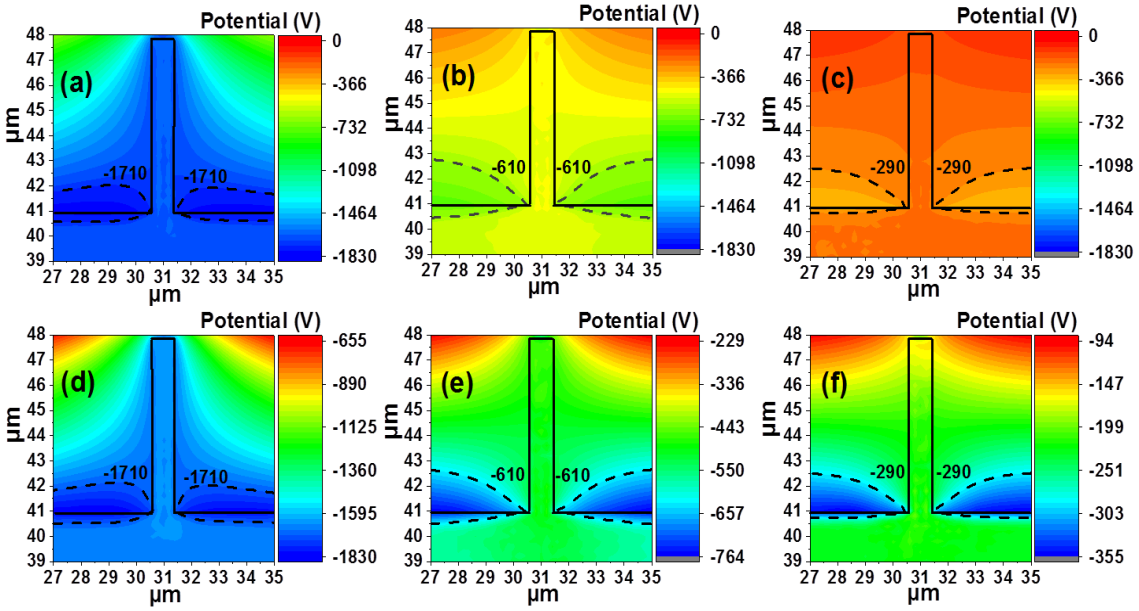

Figure 5. Electric potential distribution near and inside a pore with diameter of 800 nm, and ε_r of 4 (a,d), 50 (b,e), and 200 (c,f), at 19 ps. The black line indicates the pore. The upper panels (a-c) show

the entire range of the potential distribution (with the same color scale from 0 to –1830 V), while the lower panels (d-f) focus on the details near the pore edges (with different color scale). The dashed lines indicate a certain equipotential line (with the value indicated) to illustrate the strong potential drop near the pore entrance (see text).

3.4 Can plasma develop in pores within metallic coating?

Figure 6 shows the plasma distributions in the discharge gap (and inside the pore), for different pore sizes, in case of a metallic coating, i.e. the top dielectric is changed to metal. Note that in our simulations the entire top solid material is metallic, hence with a thickness of 9.2 μm, which represents the shell thickness in core-shell catalyst particles. Although in experiments, metallic catalysts (metal as active element) are usually dispersed in the form of ultrafine particles (mostly smaller than 10 nm), core-shell particles are also being investigated in plasma catalysis, especially to disentangle the physical and chemical effects of e.g., packing beads, i.e., bulk properties, like dielectric constant, vs. surface properties, defining the chemical reactivity of the catalyst. Hence, our simulations do not refer to the metallic catalytic nanoparticles, but rather to a metallic shell (or shell with very high dielectric constant) as being studied in core-shell particles. We will demonstrate below that the surface charging effect is the most crucial for the plasma propagation inside the pores and the horizontal spreading of plasma. Since a metal is a perfect conductor, there will be no surface charging, no matter how thick the metallic coating layer is. Besides, a metallic coating is in this context equivalent to a dielectric coating with infinite ε_r, because the polarization with infinite ε_r is so strong that there is no potential drop across the coating layer, and the conductivity of a dielectric increases with rising ε_r. Thus, the results here can reveal both the effects of a metallic coating and of a dielectric coating with infinite ε_r on the plasma distribution.

Compared to the electron density distributions in figure 1 and 2, the maximum density in the plasma bulk is now higher, due to the larger electric potential drop between the metal electrodes (i.e., -8 kV instead of around -5 kV in figure 1 and 2), as there is no potential drop across the metallic coating layer. However, as is clear from figure 6, only very limited plasma can diffuse into the pore below 1 μm diameter, even though the Debye length is only around 400 nm. With increasing pore diameter, more plasma can gradually diffuse inside the pores, but there is no discharge enhancement. The mechanism is the same as in figure 3 for $\varepsilon_r = 200$, i.e., where the surface charging effect is quite weak, due to the strong polarization at large ε_r, and the streamer propagation inside the pores becomes very difficult. In case of the metallic coating, there is no surface charging at all, and the streamer evolution inside the pore thus becomes extremely difficult, i.e. most of the plasma particles can diffuse into the pores without ionization.

Likewise, by comparing the plasma distribution inside the discharge gap of figure 6 (a) with figure 1 (c), it is obvious that the streamer width along the upper (dielectric or metallic) surface is much reduced (i.e., from 70 μm for the dielectric coating with $\varepsilon_r = 4$, to 50 μm in case of the metallic coating), indicating that the horizontal spreading of plasma is significantly suppressed by the metallic coating, as there is no surface charging. This again corresponds well with the experimental and theoretical results in [10, 24, 25, 27, 33-35], when ε_r is very large.

Therefore, the results in figure 6 further confirm that the surface charging determines both the streamer propagation inside the pores and the horizontal spreading of plasma. The metallic coating (equivalent in this context to infinite ε_r) increases the plasma density within the discharge gap, but it makes the discharge more localised.

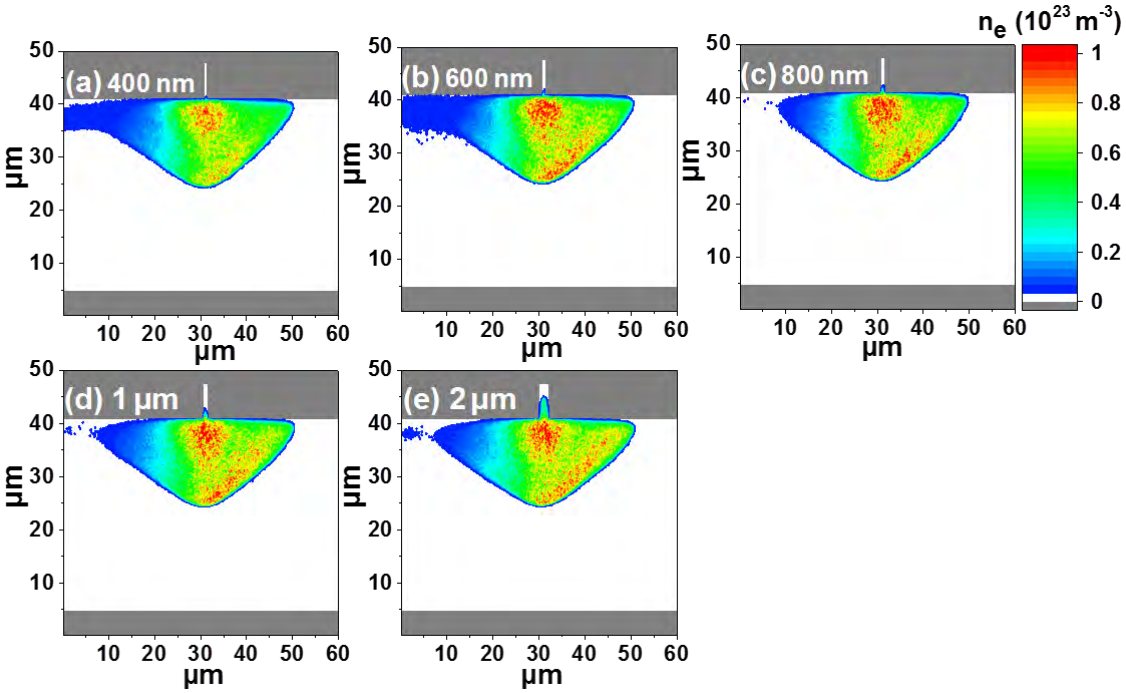

Figure 6. Plasma density distributions n_e (m^{-3}), illustrating the evolution of a plasma streamer inside the discharge and inside pores with diameter of (a) 400 nm, (b) 600 nm, (c) 800 nm, (d) 1 µm, and (e) 2 µm at 19 ps. The material at the top is metal.

Conclusions

We demonstrated that surface charging plays an important role in determining plasma streamer propagation, both in the discharge gap and inside catalyst pores, and that this effect greatly depends on the dielectric constant of the material. When ε_r is small, a surface discharge is induced by surface charging along the pore sidewalls, which enables the plasma streamer to propagate inside the pore with clear discharge enhancement. At larger ε_r (above 50), the dielectric polarization becomes more effective, which will weaken the surface charging effect and slow down the streamer propagation. The streamer length thus becomes shorter, but more electrons will accumulate near the pore entrance. Both the sharp edge and the concentrated charge density at the pore entrance give rise to a strong electric potential drop, and thus electric field enhancement near the pore entrance. The strongest electric field appears at a moderate ε_r of 50, which corresponds to the highest plasma density at the pore entrance. Hence, our simulations reveal that for pore diameters larger than the Debye length (order of 470 nm at these conditions), a plasma streamer can penetrate into catalyst pores, but the penetration is more pronounced (and thus deeper) for materials with small dielectric constant, due to enhancement by surface charging, while for materials with large dielectric constant, the plasma is more localized near the pore entrance.

In case of a metallic coating, it is very difficult for a plasma streamer to enter the catalyst pore, as there is no surface charging, and thus no surface discharge, and hence no further mechanism to accelerate the plasma streamer deeper inside the pore. The plasma distribution becomes very localised for a metallic coating, which corresponds well to experimental results from literature for extremely large values of ε_r. Therefore, we can conclude that surface charging dominates the streamer propagation inside catalyst pores, it also determines the spreading of plasma over the catalyst (dielectric) surface, and it governs the electric field strength at the sharp edges of the catalyst pores. These results help to understand the mechanisms of plasma streamer evolution inside catalyst pores in plasma catalysis.

Acknowledgments

We acknowledge financial support from the European Marie Skłodowska-Curie Individual Fellowship within H2020 (Grant Agreement 702604) and from the TOP-BOF project of the University of Antwerp. This work was carried out in part using the Turing HPC infrastructure at the CalcUA core facility of the Universiteit Antwerpen, a division of the Flemish Supercomputer Center VSC, funded by the Hercules Foundation, the Flemish Government (department EWI) and the University of Antwerp.

References

[1] E.C. Neyts, K. Ostrikov, M.K. Sunkara, A. Bogaerts, Chem. Rev. 115 (2015) 13408.
[2] H. H. Kim, A. Ogata, S. Futamura, Appl. Catal. B Environ. 79 (2008) 356.
[3] J. Van Durme, J. Dewulf, C. Leys, H. Van Langenhove, Appl. Catal. B Environ. 78 (2008) 324.
[4] H.L. Chen, H.M. Lee, S.H. Chen, Y. Chao, M.B. Chang, Appl. Catal. B Environ. 85 (2008) 1.
[5] J.C. Whitehead, J. Phys. D: Appl. Phys. 49 (2016) 243001.
[6] E.C. Neyts, A. Bogaerts, J. Phys. D Appl. Phys. 47 (2014) 224010.
[7] H. L. Chen, H. M. Lee, S. H. Chen and M. B. Chang Ind. Eng. Chem. Res. 47 (2008) 2122–30.
[8] K. Van Laer, A. Bogaerts, Plasma Sources Sci. Technol. 25 (2016) 015002.
[9] T. Butterworth, R. Elder and R. Allen Chem. Eng. J. 293 (2016) 55–67.
[10] W.Z. Wang, H.H. Kim, K. V. Laer, A. Bogaerts, Chem. Eng. J. 334 (2018) 2467–2479.
[11] U. Roland, F. Holzer, A. Poppl, F.D. Kopinke, Appl. Catal. B Environ. 58 (2005) 227.
[12] U. Roland, F. Holzer, F.D. Kopinke, Appl. Catal. B Environ. 58 (2005) 217.
[13] F. Holzer, U. Roland, F.D. Kopinke, Appl. Catal. B Environ. 38 (2002) 163.
[14] Q-Z Zhang and A Bogaerts, Plasma Sources Sci. Technol. 27 (2018) 035009.
[15] Y. Uytdenhouwen, S. Van Alphen, I. Michielsen, V. Meynen, P. Cool, A. Bogaerts, Chem. Eng. J. (2018), doi: https://doi.org/10.1016/j.cej.2018.04.210
[16] K.Takaki, K. Urashima, and J.S. Chang, IEEE Trans. Plasma Sci., 32(2004), 2175.
[17] Q. Yu, M. Kong, T. Liu, J. Fei and X. Zheng, Plasma Chem. Plasma Process. 32(2012) 153–63.
[18] I. Michielsen, Y. Uytdenhouwen, J. Pype, B. Michielsen, V. Meynen and A. Bogaerts Chem. Eng. J. 326 (2017) 477–88.
[19] U. Roland, F. Holzer, F.D. Kopinke, Catal. Today 73(2002) 315−323.
[20] F. Holzer, F.D. Kopinke, U. Roland, Plasma Chem. Plasma Process. 25(2005) 595−611.
[21] A. Mizuno, H. Ito, J. Electrost. 25 (1990) 97−107.
[22] S. Jo, T. Kim, D.H. Lee, W.S. Kang, Y.H. Song, Plasma Chem. Plasma Process. 34 (2014) 175−186.
[23] K. Van Laer and A. Bogaerts, Plasma Process. Polym. 14, (2017) e1600129.
[24] K. Van Laer, A. Bogaerts, Plasma Sources Sci. Technol. 26 (2017) 085007.
[25] T. Butterworth and R.W.K. Allen, Plasma Sources Sci. Technol. 26 (2017) 065008.
[26] K. Hensel, Eur. Phys. J. D 54 (2009) 141.
[27] H.H. Kim, Y. Teramoto, N. Negishi, A.Ogata, Catal. Today 256 (2015) 13–22.
[28] Y. Zhang, H.Y. Wang, Y.R. Zhang and A. Bogaerts, Plasma Sources Sci. Technol. 26 (2017) 054002.
[29] Retrieved on 11 June 2015 Biagi-v8.9 database www.lxcat.net.
[30] G. Lapenta, J. Comput. Phys. 181 (2002) 317–337.
[31] J. Kruszelnicki, K.W. Engeling, J.E. Foster, Z.M. Xiong and M. J. Kushner, J. Phys. D: Appl. Phys. 50 (2017) 025203.
[32] Y.R. Zhang, E.C. Neyts, A. Bogaerts, J. Phys. Chem. C 120 (2016), 25923−25934.
[33] H.J. Gallon, H.H. Kim, X. Tu, and J.C. Whitehead, IEEE Trans. Plasma Sci., 39 (2011) 2176
[34] H.H. Kim and A. Ogata, Eur. Phys. J. Appl. Phys. 55 (2011)13806
[35] H.H. Kim , Y. Teramoto, N. Negishi, A. Ogata, J. Phys. D: Appl. Phys. 49 (2016) 459501